Lab on a Chip

PAPER

View Article Online
View Journal | View Issue

Cite this: *Lab Chip*, 2026, **26**, 627

Lateral flow biosensors for low abundance detection of brain natriuretic peptide with enzyme-free amplification

Menghan Zhang, Tao Xu, Pawel Jajesniak, Giulia Core, Zhuoer Zeng, Maha Mansour Mohamed Shalaby, Julien Reboud * and Jonathan M. Cooper *

The diagnosis of heart failure in emergency settings requires rapid and sensitive detection of brain natriuretic peptide (BNP), a low-abundance biomarker of heart failure with a clinical rule-out threshold of 100 pg mL^{-1} (0.03 nM). The current gold standards for BNP testing in clinical practice all rely on immunoassays that necessitate cold-chain storage for antibodies, limiting their utility at the point-of-care. We now propose an enzyme-free, isothermal amplification strategy employing a dual-aptamer system to measure BNP at clinically relevant levels. Upon simultaneous binding to the target BNP, both of the aptamers release their complementary DNAs, consequently triggering a cyclic amplification reaction. The resulting secondary DNA structures can be detected *via* a lateral flow test (LFT) format, providing visual readouts close to the patient in 30 min at room temperature. This work advances the field by combining the specificity of aptamers with the simplicity of LFTs, offering the sensitivity of conventional immunoassays while eliminating any enzymatic steps. This work bridges the gap between lab-based immunoassays and POC needs, offering a reliable, equipment-free alternative for heart failure diagnosis in resource-limited settings. Future studies will validate its performance with blood samples for clinical deployment.

Received 13th August 2025,
Accepted 26th December 2025

DOI: 10.1039/d5lc00793c

rsc.li/loc

Introduction

Heart failure remains the primary cause of mortality worldwide, imposing the highest cost on the healthcare sector.[1] Brain natriuretic peptide (BNP) is the gold-standard biomarker for managing heart failure due to its high negative predictive value.[2,3] Normal levels of BNP (<100 pg mL^{-1}) can be 98% accurate for excluding heart failure in emergency settings,[4] permitting the development of tests that can rule out heart failure in symptomatic patients. To enable its use at the point-of-care (POC), BNP tests also need to be rapid (result within 30 minutes), allowing for timely clinical decision-making at the patient's bedside or in outpatient settings.[5] Such a test could help streamline the diagnostic process, reducing the need for unnecessary hospital admissions and thus improve resource utilization.[6]

BNP is a neurohormone secreted in response to overloaded ventricular stress to maintain cardiovascular homeostasis, so that its levels directly correlate with the severity of heart failure, making it a highly specific biomarker for diagnosing and monitoring this condition.[2,7] Optical sensors for BNP, using fluorescence or chemiluminescence, Raman spectroscopy, and surface plasmon resonance have achieved ultra-high sensitivity down to 50 pg mL^{-1} – although generally these lab-based methods require bulky and costly instrumentation.[8] Electrochemical BNP sensors are self-contained combined devices that can be more easily miniaturized. However, nonspecific binding, as well as the need for costly redox reagents and significant expertise, have limited their application in POC for BNP.[9]

Existing lab-based immunoassays for BNP POC testing require dedicated devices or analyzers, which leads to challenges in bringing the testing capabilities close to the patient, outside of centralised laboratories, while maintaining the high performance levels required for clinical decision-making.[10] Assays under development have aimed to improve specificity, although they are challenged by the substantial cross-reactivities between BNP and other metabolites of the BNP precursor (proBNP).[11,12] BNP antibody-based immunoassays integrated with high-precision detection platforms are currently the most specific and sensitive BNP biosensors, reaching limits of detection (LoDs) down to 1 pg mL^{-1}.[12] Nevertheless, the clinical translation of BNP sensing to POC platforms is constrained by long turnaround times and environment-related challenges such as storage temperature or humidity.[13]

Aptamers, as nucleic acids, offer useful alternatives to antibodies, with higher stability under a wider range of

University of Glasgow, University Avenue, Glasgow, G12 8QQ, UK.
E-mail: julien.reboud@glasgow.ac.uk, Jon.Cooper@glasgow.ac.uk

environmental conditions, while still binding to target molecules with comparable affinity and specificity.[8,14] In this work, we address the abovementioned limitations with two aptamers targeting different epitopes on the BNP molecule to achieve higher specificity by lowering the risk of cross-reactivity with other related peptides from the blood sample, such as NT-proBNP and proBNP.[15] A dual-aptamer system could also minimise interference by ensuring that only the target BNP molecule is captured and detected, thereby enhancing the robustness of this POC testing. The use of aptamers further allows the coupling of an isothermal nucleic acid-based amplification reaction for high sensitivity, in this case involving a catalytic hairpin assembly (CHA) as a non-enzymatic assay.[16] Such an assay provides benefits brought by the use of aptamers, with longer shelf life/higher stabilities and simplified workflows.[17] While enzymatic reactions can introduce variability due to differences in enzyme activity, substrate availability, or reaction kinetics, we aim to improve reproducibility with an enzyme-free assay.[18]

Thus, we introduce a new BNP assay strategy in a lateral flow test (LFT) format that is easy-to-use, easy-to-read, and more economical for widespread use in POC settings. Inspired by non-competitive enzyme-linked immunosorbent assay (ELISA), in which the target is sandwiched between a capture and a detection antibody,[19] we show the development of a DNA circuit incorporating a pair of BNP aptamers that recognise the same target in parallel but at different epitopes.[20,21] This new design creates a homogeneous detection assay for BNP using a matched aptamer pair (Fig. 1A).

The binding event triggers amplification through a CHA strategy in an isothermal and enzyme-free reaction (Fig. 1B).[22] Recruiting more than one single affinity probe enhances the detection specificity, whilst isothermal enzyme-free amplification provides the ability to incorporate the process in simple biosensors,[23] here using LFT strips for rapid and equipment-free visual readouts.[24]

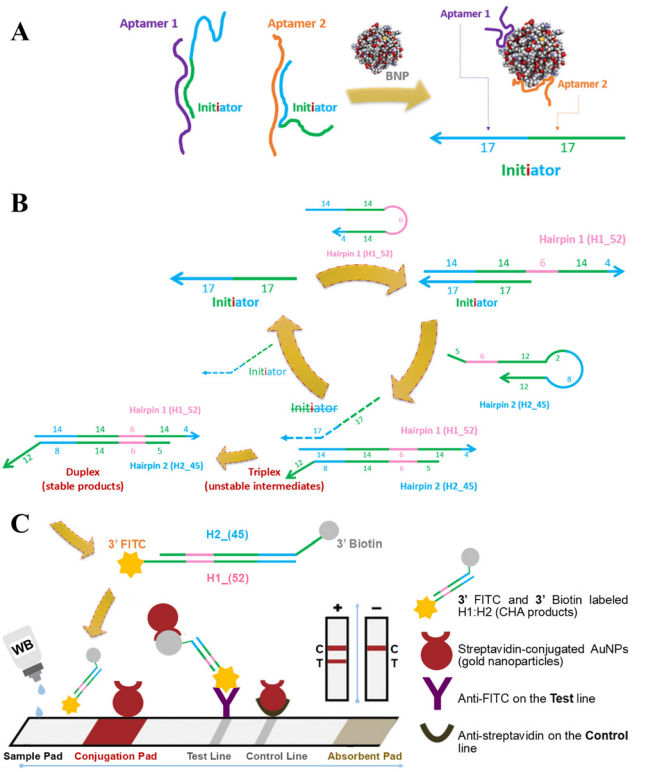

Fig. 1 Schematic illustration of BNP biosensing *via* CHA reaction circuit. (A) Pre-initiation phase, the initiator is insulated by dual aptamers in a single pot to prevent self-activation, as it is designed to be partially complementary with both aptamer 1 and aptamer 2 (binding sites separated by the red 'i' in the figure for visual emphasis). (B) BNP-induced and dual aptamers binding-catalysed hairpin assembly and disassembly cascades, triggered by the released initiators. The number marks the length (in nucleo) of each segment corresponding to the colour coding, which is consistent with the design of the sequences (colour matching means either complementary or sequences derived from the same source). (C) LFT integration with sample loading onto the test strips for biosensing of the CHA signal, followed by two drops of the washing buffer (WB, *ca.* 54 μL). The FITC/biotin-labeled hairpin duplexes are captured by anti-FITC antibodies at the test line, indicative of the presence of the marker.

Results and discussion

Characterisation of CHA signal on nPAGE

We selected two existing BNP aptamer sequences with the least cross-competition that both undergo conformational changes when binding with BNP.[21] This strategy releases complementary DNA sequences (initiators), previously *hidden* by both aptamers, which are then able to bind to other components of the CHA circuit (Fig. 1B). In the reaction pathway, CHA is initiated by a single-strand DNA initiator, which can sequentially open two participating hairpins *via* the toehold-mediated strand displacement.[17,25] The signal is accumulated while the cascading CHA disassembles more and more hairpin 1 (H1) and hairpin 2 (H2) into H1 : H2 duplexes. The H1 functions as the molecular beacon (H1MB) when modified with fluorescein isothiocyanate (FITC) on the 5′ end and black hole quencher 1 (BHQ1) on the 3′ end to ensure quenching of the fluorophore when H1 was properly folded at the initial stage. In our new design, initiators trigger the CHA reaction only after both aptamers (aptamer 1 and aptamer 2) are bound to BNP as the conformational recognition changes their shapes to displace the initiators from the aptamer pairs (Fig. 1A). Experimentally, the proposed CHA cascade integrating dual aptamers was validated through native polyacrylamide gel electrophoresis (nPAGE), while performance of the CHA was evaluated by fluorescence intensities of the product band. Analysis of the CHA signal from the nPAGE images was done by ImageJ for fluorescence quantification, which was also confirmed by H1MB fluorescence.

In Fig. 2A, the band intensities of CHA products in lanes 2–11 showed that the products built up with decreasing levels of aptamer 1&2. No breathing effect of the hairpins was observed from the lane 12, as H1 and H2 failed to open each other in the absence of initiators, indicating that there was

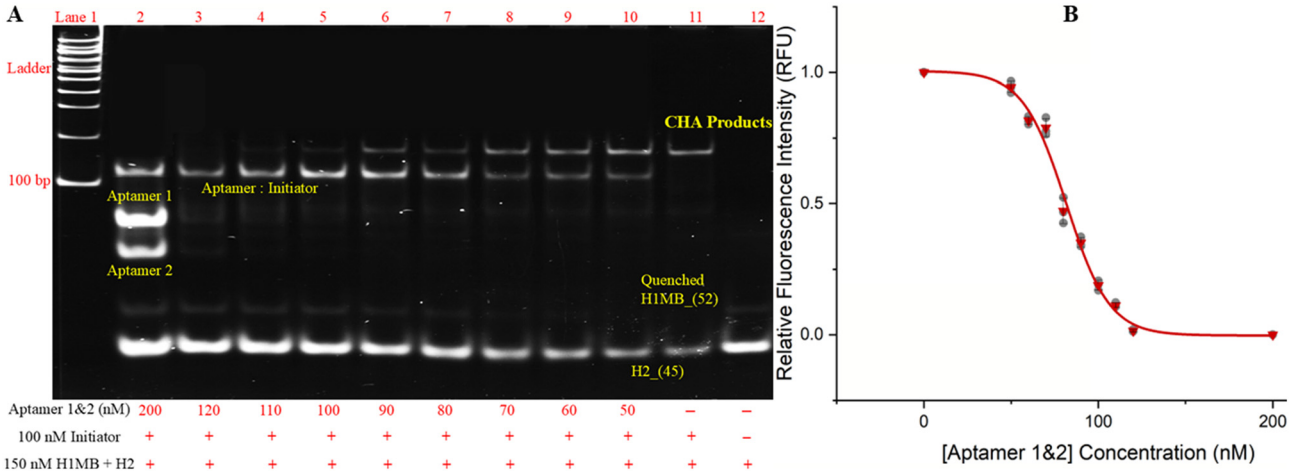

Fig. 2 Characterisation of CHA reaction final products by nPAGE. (A) nPAGE image of CHA performance supplied with decreasing levels of aptamer 1&2, the text in yellow indicates the bands of the expected size. Lane 12 suggests there is no circuit leakage given no-show of spontaneous hybridisation products when 150 nM of H1 and H2 are mixed together; lane 11 is the positive control when there is no aptamers, the initiators are free to trigger the CHA circuit; lane 2 is the negative control when the [initiators] : [aptamer 1&2] are added in a 1 : 2 ratio, all the initiators are detained from the CHA activation, and thus the product band disappears. The two bands appearing at the bottom in every lane are the surplus H1 and H2, with the brighter one being H2 because the unconsumed H1 is still folded and quenched by BHQ1. Lane 1 is a 100 bp ladder. (B) Plot of the quantitated band intensities, with standard deviation of each set of triplicate results as the error bars. The Boltzmann fit (also known as the 4-parameter logistic fit) of the means reports an R^2 of 0.992, and an X_0 of 81.57 as the inflection point of the sigmoidal curve, and the regression is predicted as $y = -0.003 + 1.008/\{1 + \exp[(x - 81.568)/12.393]\}$.

no circuit leakage.[26] When the aptamer pair was introduced with decreasing concentration, the intensity of the bands created by the reactions increased. The band of CHA products disappeared from lane 2 and 3 when aptamer 1&2 were supplied in excess to saturate all the free initiators. Beyond the 1.2 : 1 ratio of [aptamer 1&2] : [initiators], aptamer 1&2 are abundant enough to capture all the initiators, hence inhibiting the activation of CHA reaction. Aptamer 1 : initiator and aptamer 2 : initiator duplexes end up at the same position after gel electrophoresis (demonstrated by lane 12 and 13 in Fig. S1). These appear as the topmost band in lane 2, which intensified as more aptamer 1&2 was added to bind with the initiators. The band intensities of the remaining H1 and H2 also demonstrate that the less aptamer 1&2, the more CHA reactions were triggered as more initiators were released to assemble the final product of H1 : H2 duplexes, so that less hairpins are left. The mean signals of CHA products were fitted into a Boltzmann curve (Fig. 2B, also known as the 4-parameter logistic curve). The fit supports the finding that to manipulate the CHA signal effectively, the concentration of aptamer 1&2 needs to be comparable to that of the initiators (more details about the Boltzmann curve and relevance to fitting and analysis are provided in SI).[27]

Homogeneous CHA using fluorescence

As confirmation of the reaction mechanism, the CHA signal was monitored through fluorescence reading of FITC on a H1MB probe. For each one-pot reaction, both H1MB and H2 were supplied at 150 nM in a 1 : 1 ratio. Fig. 3A shows a similar reaction profile when varying the concentrations of the initiators. To ensure a broader responsive range, the input of initiators was kept constant at 100 nM while varying aptamer 1&2. This approach by fluorescence reading returns an inflection point at around 90 nM (x_0, inflection point in blue, Fig. 3A), consistent with the 82 nM from the nPAGE analysis (x_0, Fig. 2A). Given the supply of both hairpins at 150 nM, the curve for initiators turns to be steepest at 43.9 nM (inflection point in orange), and dual aptamers at 90.9 nM. This approximate ratio of 2 : 1 ([aptamer 1&2] : [initiator]) can serve as a guideline of the critical amount of aptamers and initiators needed in order to make the CHA signal most sensitive to fluctuations in the predictor variable.

The initiators that are bound by either aptamer will not be able to participate in any downstream reactions, whereas only unbound initiators will be free to set off the CHA. The relative fluorescence intensities of H1MB signify the number of H1MB unzipped and contributed to the CHA, which can be used to predict the remainders that are not involved. Since the starting concentrations of initiators are the same and the fluorescence signals were all calibrated by the CHA reaction supplied with 100 nM of free initiator, any decline in signal in the presence of aptamer 1&2 can be ascribed to binding-induced suppression of the CHA.

This approach allowed us to provide concentrations of the bound and free initiators, from which the binding curve can be plotted accordingly (Fig. 3B). The green curve illustrates the fact that less [initiators] will be free if the concentration of [aptamer 1&2] rises. On the contrary, the purple curve in Fig. 3B depicts that more [initiator : aptamers] complexes will be formed as [aptamer 1&2] increases. To quantitatively analyse the binding interaction between the initiator and the dual aptamers, the

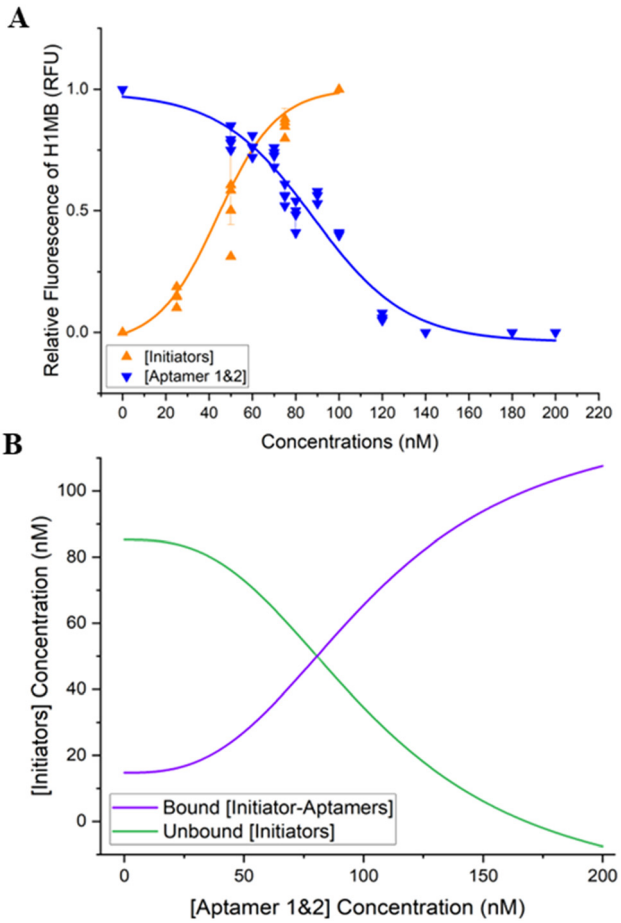

Fig. 3 Fluorescence measurements of CHA signal *via* hairpin probe H1MB. The fluorescence readouts were calibrated by signal from the positive control (100 nM initiator + 150 nM H1MB + 150 nM H2) after subtracting the background signal (150 nM H1MB + 150 nM H2). (A) The Boltzmann curve in orange describes the changes in CHA signal with regards to increasing concentrations of initiator from 0 to 100 nM, given constant source of H1MB and H2 both at 150 nM, with an R^2 of 0.998 and an x_0 of 43.9; the Boltzmann curve in blue depict the range of CHA signal responding to 0–200 nM of aptamer 1&2, provided with 100 nM of initiators and 150 nM of hairpins, with an R^2 of 0.976 and an x_0 of 90.9. Error bars are standard deviations of triplicate results. (B) At the same value of y (relative fluorescence of H1MB), two x values (concentrations of [initiators] and [aptamer 1&2]) can be derived from (A), and the two corresponding x values are plotted as shown by the green sigmoidal curve in (B); where the [initiators] are free to open H1MB to signal, the rest [initiators] bound by the [aptamer 1&2] can also be plotted to scrutinise the binding curve between them as illustrated by the purple sigmoidal curve. The fit-ted Hill equation reports a K_d value of 104.52 and a Hill coefficient (n) of 2.78, with an R^2 of 0.994.

data were fitted to the Hill equation (purple curve, R^2 = 0.994), noting that the binding between initiator and aptamers does not start at 0 nM of initiators (analysis with the Hill equation is presented in details in SI). Given the Hill equation from Fig. 3B, a Hill coefficient (parameter n) of 2.78 specifies the degree of cooperativity, where $n > 1$ indicates positive cooperativity.[28] This could indicate that there is more than one site on the initiator for aptamer binding, and the binding of one aptamer enhances the affinity of other binding sites on the same initiator for the second aptamer to bind. This corresponds to the design of the initiator (listed in Table S1) as its 5′ half is designed to be complementary to the recognition region within aptamer 2, with its 3′ half complementing the recognition segment of aptamer 1.[21]

Conversely the sigmoid in purple revealed that at minimal [aptamer 1&2] concentrations, initial binding occurs slowly because few [initiators] are bound, and at maximal [aptamer 1&2] concentrations, the response approaches saturation as the binding sites are mostly occupied. The system responds most dynamically to variations in [aptamer 1&2] concentration when it is partially saturated, *i.e.*, halfway between the START (15 nM, baseline response) and END values (123 nM, plateau response). This is calculated to be *ca.* 70 nM of [initiators] when the system achieves its highest sensitivity.[29] Furthermore, parameter k from the Hill equation (Fig. 3B) refers to the dissociation constant, suggesting that half of the [initiators] would be bound once the concentration of [aptamer 1&2] reaches 105 nM. Experimentally, each aptamer binds with the initiator in a 1 : 1 fashion, and so [aptamer 1&2] concentration needs to be doubled in order to capture the same amount of [initiators].

Using a threshold background as 3 times the standard deviation of the baseline, 0.10 a.u. for nPAGE and 0.09 a.u. for the one-pot fluorescence, allowed us to determine a corresponding limit of detection (LoD) of [aptamer 1&2] as 108 nM and 124 nM, respectively. In acute settings, the BNP LoD should be below 100 pg mL^{-1}, corresponding to 0.03 nM (ref. 1 and 7) and thus we adopted the LFT format to detect the interaction between aptamers and BNP to reach this important metric.

Optimisation on LFT strips

H1 was modified with 3′FITC, and H2 with 3′Biotin, such that only the H1 : H2 hybrid can be captured onto the test line of a commercial strip, containing an anti-FITC antibody,[24] whilst the control line hosts an anti-streptavidin antibody to capture streptavidin-gold particles flowing with the sample. Aiming for a visual signal down to 0.03 nM of BNP required at least 0.06 nM of aptamer 1&2. We first minimized the leakage signal on LFT strips which suggested that any levels of H1 and H2 above 0.14 nM will generate a false positive signal even in the absence of initiators (see SI Note in SI). Fig. 4A shows that at 0.14 nM of H1 and H2, the background leakage caused by spontaneous hybridisation between hairpins was not observed, whereas the signal appeared at the test line if 0.06 nM of initiators was supplied. Decreasing concentrations of aptamer 1&2 from 0.24 nM down to 0.10 nM, showed no test line signal as most initiators were sequestered by aptamers. In contrast, as soon as the BNP level rose to an extent that the accessible aptamer 1&2 fell under 0.10 nM, the CHA signal re-appeared as those released initiators become abundant enough for CHA activation. In this case, 0.10 nM of aptamer 1&2 is considered the LoD of LFT with a linear relationship above (R^2 = 0.930, Fig. 4B). The

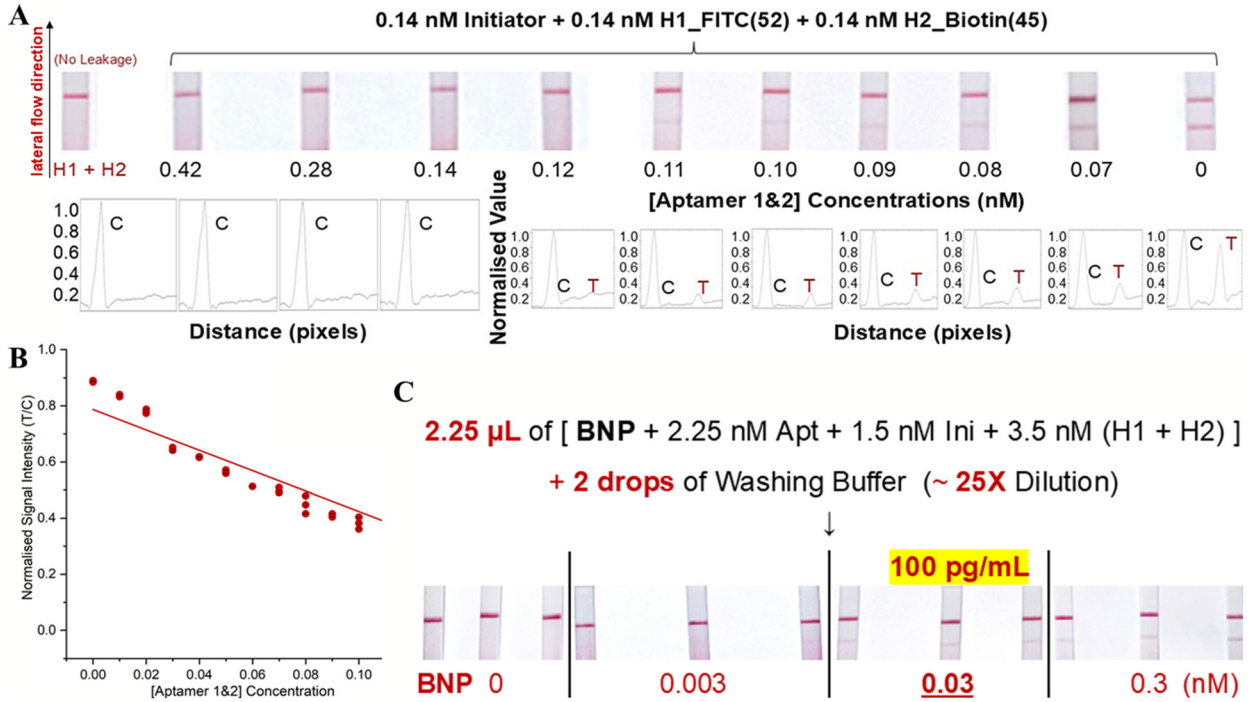

Fig. 4 Biosensing of CHA signal on LFT strips, where each result is representative of three independent LFT measurements (n = 3). (A) Visualisation of LFT results and signals quantified; first strip is the negative control, indicating no leakage signal when there are only H1 (3′FITC) and H2 (3′Biotin), whilst the last strip is the positive control, showing that the test line is the strongest when the [aptamer 1&2] concentration is 0 nM; the test line disappears when the [aptamer 1&2] is beyond 0.10 nM. (B) Relative optical density of the test-line signals standardised by that of the control-line signals, the linear equation is fitted across the triplicate LFT results from 0–0.10 nM of [aptamer 1&2] (as the test signal disappears beyond 0.10 nM), with an R^2 of 0.930 and the standard deviations being the error bars. (C) LFT integration with sample loading onto the test strips for biosensing of the CHA signal, followed by two drops of the washing buffer (WB, *ca.* 54 µL) for the ease of dilution. The FITC/biotin-labeled hairpin duplexes are captured by anti-FITC antibodies at the test line, with digital responses of the LFT achieved at the BNP threshold after dilution with the WB.

linear correlation between [aptamer 1&2] concentrations and signal intensity could also serve as a calibration for monitoring of BNP levels among patients with chronic heart failure for prognosis.[30] For a POCT device, a one-pot reaction with a binary output is preferred, where "0" indicates a BNP level below a clinically relevant threshold (lower than 100 pg mL^{-1}) and "1" above. From the BNP binding assay (see SI), we determined the K_d between BNP and the two aptamers to be *ca.* 14 nM. With the concentration of BNP and aptamers being 0.03 nM and 0.10 nM, the bound aptamer-BNP concentration would be as low as 0.21 pM approximately, suggesting that formation of aptamer-BNP complexes is extremely limited. The K_d value implies that the supply of free aptamer and BNP should approach 14 nM for the binding events to be significant. An LFT visual response for 0.03 nM of BNP occurred for optimised concentrations [aptamers (2.25 nM), initiators (1.5 nM), and hairpins (3.5 nM)] (Fig. 4C).

The dissociation constant for the interaction between BNP and our dual-aptamer system was 14 nM. In comparison, existing panel of BNP aptamers reported K_d values stretching from 12.5 to 139 nM,[31] placing our system within a competitive range, while offering the added advantages of enzyme-free amplification and LFT compatibility. Although other systems, including antibodies for example, can have much better K_d values (*e.g.* 1.0 ± 0.4 nM and 0.33),[32,33] when coupled with CHA, it is sufficient to achieve a clinically relevant LoD of 0.03 nM, as the reaction amplifies the signal from even a small number of initiators released from the aptamer binding events.

Moreover, our dual-aptamer approach enhances specificity by targeting distinct epitopes simultaneously, thereby reducing off-target binding and the likelihood of cross-reactivity with related peptides such as NT-proBNP, which is a common source of false positives in single-probe BNP assays.[34]

While the commercial LFT strips employ anti-FITC and anti-streptavidin antibodies for signal capture, these are used solely for universal reporter detection and do not interact with BNP. They have been extensively developed to enable lyophilisation onto the nitrocellulose membranes. Such a process is challenging to carry out for new markers as it requires lengthy and prohibitive optimisations, which aptamers are able to circumvent.

Experimental

Materials

Both sequences of the aptamers against BNP were selected from an aptamer-based ELISA-like microplate assay[21]

(sequences listed in Table S1). All DNA oligonucleotides used in this study were purchased from IDT (Integrated DNA Technologies, Inc., Coralville, Iowa), with HPLC purification. Human BNP (1–32, Cat. No. 3522) was purchased from Tocris (Bio-Techne Ltd., UK). 40% acrylamide/bis-acrylamide solution 29 : 1, TEMED, and ammonium persulfate (APS) were purchased from Bio-Rad (Bio-Rad Laboratories Ltd., UK). UltraPure™ 10× TBE buffer (Tris-boric-EDTA), 6× DNA gel loading dye, SYBR™ Gold, and UltraPure™ DNase/RNase-free distilled water were obtained from Invitrogen (ThermoFisher Scientific). Reaction buffer (pH 8.0, 5 mM Tris-HCl, 0.5 mM EDTA, 100 mM NaCl, 20 mM KCl and 50 mM $MgCl_2$) was kept unchanged for all the different experiments described to sustain the optimal buffered conditions for catalytic efficiency. Low volume 384-well microplates (black, flat bottom) were purchased from Corning (Corning Life Sciences). LFT strips were ordered from Ustar Biotechnologies Ltd. (U-Star Disposable Nucleic Acid Detection Strips, Type 3; Hangzhou, Zhejiang, China).

Design of CHA sequences and characterisation of CHA thermodynamics

The initiator (34 nt) sequence was adapted from the BNP aptamer sequences, with its 5′ half partially complementary to the aptamer 2 sequence, and its 3′ half partially complementary to the aptamer 1 sequence. H1 (52 nt) was designed with a hairpin stem of 18 bp, and a loop of 6 nt, with a 10 nt single-strand overhang serving as the toehold region for hybridisation with the initiator. H2 (45 nt) was designed with a 12 bp stem, a 10 nt hairpin loop, and an 11 nt overhang as the toehold to hybridise with the H1. Once opened, the duplex of H1 : initiator has 28 bp and H1 : H2 has 33 bp being fully complementary. The length of each CHA building block has been adjusted so that the differences in molecular weight of the designed DNA sequences could be clearly distinguishable on a 15% nPAGE.

The Gibbs free energy (ΔG) of hairpin formation and its melting temperature (Tm) were predicted using OligoAnalyzer™ tool.[35] Likewise, the ΔG for each bimolecular interaction among combinations of the initiator, H1, H2, aptamer 1, and aptamer 2 was also analysed through the hetero-dimers function of OligoAnalyzer™ tool (detailed in Fig. S2). For each possible dimerisation, the Tm needs to be well above room temperature ($\gg$25 °C), whilst the ΔG needs to be negative for the CHA reaction to proceed spontaneously. Considering the hybridisation stability of each duplex, the length of the complement and the GC content have also been accommodated for the CHA reaction to operate optimally below the Tm,[36] *i.e.*, under its Tm, H1 would be in a partially folded state, allowing interactions with the initiator strand and H2 subsequently.

Renaturation of hairpins and one-pot CHA

Hairpin samples were reconstituted from stock solutions to desired concentration (600 nM) in reaction buffer. Then the hairpin sample was heated to 90–95 °C for 10 minutes to fully denature any secondary structures, followed by gradual cooling at a rate of 0.02 °C s^{-1} down to room temperature in a thermal cycler, over the course of 1 hour. This allowed the H1 and H2 to reform in their most stable and intended configuration. The hairpin samples were stabilised at the final temperature (25 °C) for an additional 15 min to ensure complete and steady renaturation.[37] All the CHA reaction mixtures ended up with a total volume of 40 μL containing the initiator, H1 and H2 in a 1 : 1 ratio, and the aptamer 1&2 or not in the reaction buffer. The final concentrations of both hairpins (150 nM, 10 μL each) and initiators (100 nM, 10 μL) were held constant across the reactions while the aptamer 1&2 (10 μL) concentrations changed: 0 nM, 50 nM, 60 nM, 70 nM, 80 nM, 90 nM, 100 nM, 110 nM, 120 nM, 200 nM. The reaction tube was incubated for 30 minutes at room temperature (see Fig. S4 for optimisation data).

Non-denaturing gel electrophoresis

nPAGE was used to evaluate the performance of the CHA, where the appearance and intensity of new bands were studied to assess the interactions among the CHA components and how they were regulated by changing inputs. For each individual reaction mixture, the DNA solutions (10 μL) were mixed with 6× DNA loading buffer (2 μL) before loading into the 15% nPAGE (casted from 40% (w/v) acrylamide/bis-acrylamide solution 29 : 1). The electrophoresis was run in 1× TBE buffer (pH 8.0) at a constant voltage of 110 V for 90 minutes. The gels were imaged using Syngene PXi (Syngene, Frederick, MD) after staining with SYBR Gold (dsDNA and ssDNA dye) for 5 minutes. Imaging parameters were set as follows: UltraSlim – blue light transilluminator (excitation) and Filt 525 nM (emission), with an exposure time of 800 ms.

Fluorescence-based measurement

The fluorescent intensities of FITC-functionalised H1MB were read from the bottom of 384 well plates by the Synergy™ HT Gen5 Microplate Reader (BioTek® Instruments, Inc., Agilent, Santa Clara, California, United States) with the filter set of 485/20 nm and 528/20 nm for excitation and emission. Data were collected every minute.

Optimisation of dual-aptamer regulated CHA signal on LFT

To visualise the CHA signal on LFT strips, FITC and biotin were respectively incorporated onto the 3′ ends of H1 and H2. After CHA (30 min), 2.25 μL reaction mixtures from each sample were deposited on LFSs, with 54 μL of the running buffer from the manufacturer (Ustar Biotechnologies Ltd.) to move the sample through the test and control lines (see Fig. S5 for optimisation data of the washing buffer volume). After 10 minutes, the LFT outcomes were imaged.

Conclusions

We present a novel BNP assay that employs dual aptamers to associatively trigger non-enzymatic nucleic acid-based cascades. In the presence of target BNP, the aptamer pair can coordinate the reaction circuit through the release of a single initiator. A key advantage of this one-pot format is the potential for application at POC. Incubation is as rapid as a lateral flow test, up to 30 minutes at room temperature. By porting the system onto a LFT strip, we established the possibility of POC BNP testing at the clinical significance level. Our novel BNP assay avoids the use of any antibody or enzymes for target recognition and signal amplification, while the dual BNP aptamers approach provides potential for high selectivity, generating a viable prototype for the POC diagnostics of BNP with clinically significant cut-off values. This assay targets whole blood/serum to align with the emergency department workflows, and so the future work will focus on the validation of this developed test with clinical samples.

Author contributions

MZ: conceptualisation, formal analysis, investigation, methodology, project administration, validation, writing – original draft. TX: methodology, data curation, software. PJ: methodology, resources. GC: methodology, project administration. ZZ: investigation, validation. MMMS: methodology. JR: funding acquisition, project administration, supervision, writing – review & editing. JMC: funding acquisition, supervision, writing – review & editing.

Conflicts of interest

There are no conflicts to declare.

Data availability

All data supporting the findings of this study are available within the paper and supplementary information (SI). Additional datasets, including raw gel electrophoresis images, fluorescence intensity measurements, and lateral flow test results analysed during the current study are available open access at Glasgow University repository at DOI: https://doi.org/10.5525/gla.researchdata.1961.

Supplementary information is available. See DOI: https://doi.org/10.1039/d5lc00793c.

Acknowledgements

This work was supported by the China Scholarship Council, the UKRI (NE/V010085/1) and the Engineering and Physical Sciences Research Council (2900683), as well as by scholarship funding from the Egyptian Ministry of Higher Education [MM28/19].

References

1 H. Alawieh, T. El Chemaly, S. Alam and M. Khraiche, Towards Point-of-Care Heart Failure Diagnostic Platforms: BNP and NT-proBNP Biosensors, *Sensors*, 2019, **19**(22), 5003.
2 R. A. Booth, S. A. Hill and A. Don-Wauchope, *et al.*, Performance of BNP and NT-proBNP for diagnosis of heart failure in primary care patients: a systematic review, *Heart Failure Rev.*, 2014, **19**(4), 439–451.
3 M. Weber and C. Hamm, Role of B-type natriuretic peptide (BNP) and NT-proBNP in clinical routine, *Heart*, 2006, **92**(6), 843–849.
4 N. Shimizu and K. Kotani, Point-of-care testing of (N-terminal pro) B-type natriuretic peptide for heart disease patients in home care and ambulatory care settings, *Pract. Lab. Med.*, 2020, **22**, e00183.
5 J. Mair, G. Falkensammer, G. Poelzl, A. Hammerer-Lercher, A. Griesmacher and O. Pachinger, B-type natriuretic peptide (BNP) is more sensitive to rapid hemodynamic changes in acute heart failure than N-terminal proBNP, *Clin. Chim. Acta*, 2007, **379**(1), 163–166.
6 E. Roberts, A. J. Ludman and K. Dworzynski, *et al.*, The diagnostic accuracy of the natriuretic peptides in heart failure: systematic review and diagnostic meta-analysis in the acute care setting, *BMJ [Br. Med. J.]*, 2015, **350**, h910.
7 C. J. Taylor, J. M. Ordóñez-Mena and S. L. Lay-Flurrie, *et al.*, Natriuretic peptide testing and heart failure diagnosis in primary care: diagnostic accuracy study, *Br. J. Gen. Pract.*, 2023, **73**(726), e1–e8.
8 O. A. Goryacheva, T. D. Ponomaryova and D. D. Drozd, *et al.*, Heart failure biomarkers BNP and NT-proBNP detection using optical labels, *TrAC, Trends Anal. Chem.*, 2022, **146**, 116477.
9 E. C. Wilkirson, K. L. Singampalli and J. Li, *et al.*, Affinity-based electrochemical sensors for biomolecular detection in whole blood, *Anal. Bioanal. Chem.*, 2023, **415**(18), 3983–4002.
10 I. Sarangadharan, S.-L. Wang and T.-Y. Tai, *et al.*, Risk stratification of heart failure from one drop of blood using hand-held biosensor for BNP detection, *Biosens. Bioelectron.*, 2018, **107**, 259–265.
11 A. G. Semenov and E. E. Feygina, in *Advances in Clinical Chemistry*, ed. G. S. Makowski, Elsevier, 2018, pp. 1–30.
12 N. N. Tamm, K. R. Seferian and A. G. Semenov, *et al.*, Novel Immunoassay for Quantification of Brain Natriuretic Peptide and Its Precursor in Human Blood, *Clin. Chem.*, 2008, **54**(9), 1511–1518.
13 D. J. Lee and T.-C. Aw, Natriuretic peptides in clinical practice: a current review, *J. Immunol. Sci.*, 2023, **7**, 28–34.
14 A. Mahmud, D. Chang and J. Das, *et al.*, Monitoring Cardiac Biomarkers with Aptamer-Based Molecular Pendulum Sensors, *Angew. Chem., Int. Ed.*, 2023, **62**(20), e202213567.
15 A. S. Al-Ibrahimi, M. E. Al-Gazally and M. M. Alshok, Biochemical analysis of the natriuretic peptides BNP and NT-proBNP in patients with cardiovascular disease, *Int. J. ChemTech Res.*, 2016, **9**(12), 508–519.
16 A. M. Kabza and J. T. Sczepanski, l-DNA-Based Catalytic Hairpin Assembly Circuit, *Molecules*, 2020, **25**(4), 947.

17 Z. Luo, Y. Li and P. Zhang, *et al.*, Catalytic hairpin assembly as cascade nucleic acid circuits for fluorescent biosensor: Design, evolution and application, *TrAC, Trends Anal. Chem.*, 2022, **151**, 116582.
18 M. Zou, F. Su and R. Zhang, *et al.*, Rapid point-of-care testing for SARS-CoV-2 virus nucleic acid detection by an isothermal and nonenzymatic Signal amplification system coupled with a lateral flow immunoassay strip, *Sens. Actuators, B*, 2021, **342**, 129899.
19 C. Ferreira, K. Papamichael, G. Guilbault, T. Schwarzacher, J. Gariepy and S. Missailidis, DNA aptamers against the MUC1 tumour marker: design of aptamer–antibody sandwich ELISA for the early diagnosis of epithelial tumours, *Anal. Bioanal. Chem.*, 2008, **390**, 1039–1050.
20 J. G. Bruno, Integration of multiple computer modeling software programs for characterization of a brain natriuretic peptide sandwich DNA aptamer complex, *J. Mol. Recognit.*, 2019, **32**(12), e2809.
21 J. G. Bruno, A. M. Richarte and T. Phillips, Preliminary Development of a DNA Aptamer-Magnetic Bead Capture Electrochemiluminescence Sandwich Assay for Brain Natriuretic Peptide, *Microchem. J.*, 2014, **115**, 32–38.
22 Y. Jiang, B. Li, J. N. Milligan, S. Bhadra and A. D. Ellington, Real-Time Detection of Isothermal Amplification Reactions with Thermostable Catalytic Hairpin Assembly, *J. Am. Chem. Soc.*, 2013, **135**(20), 7430–7433.
23 W. Wang, A. Nie, Z. Lu, J. Li, M. Shu and H. Han, Catalytic hairpin assembly-assisted lateral flow assay for visual determination of microRNA-21 using gold nanoparticles, *Microchim. Acta*, 2019, **186**(9), 661.
24 J. Reboud, G. Xu and A. Garrett, *et al.*, Paper-based microfluidics for DNA diagnostics of malaria in low resource underserved rural communities, *Proc. Natl. Acad. Sci. U. S. A.*, 2019, **116**(11), 4834–4842.
25 W. Dai, J. Zhang and X. Meng, *et al.*, Catalytic hairpin assembly gel assay for multiple and sensitive microRNA detection, *Theranostics*, 2018, **8**(10), 2646–2656.
26 X. Han, H. Yu and L. Zhang, *et al.*, Movable toehold for leakless self-assembly circuits, *Biosens. Bioelectron.*, 2024, **245**, 115823.
27 M. Zou, M. Zhou and S. Ma, *et al.*, Addition of dNTPs can improve the detection sensitivity of catalytic hairpin assembly, *iScience*, 2023, **26**(4), 106390.
28 G. Ortega, D. Mariottini, A. Troina, F. W. Dahlquist, F. Ricci and K. W. Plaxco, Rational design to control the trade-off between receptor affinity and cooperativity, *Proc. Natl. Acad. Sci. U. S. A.*, 2020, **117**(32), 19136–19140.
29 B. K. Verma, A. A. Mannan, F. Zhang and D. A. Oyarzún, Trade-Offs in Biosensor Optimization for Dynamic Pathway Engineering, *ACS Synth. Biol.*, 2022, **11**(1), 228–240.
30 M. Oremus, A. Don-Wauchope and R. McKelvie, *et al.*, BNP and NT-proBNP as prognostic markers in persons with chronic stable heart failure, *Heart Failure Rev.*, 2014, **19**(4), 471–505.
31 Y. Wang, J. Wu and Y. Chen, *et al.*, Magnetic microparticle-based SELEX process for the identification of highly specific aptamers of heart marker-brain natriuretic peptide, *Microchim. Acta*, 2015, **182**(1), 331–339.
32 S. Y. Tetin, Q. Ruan and J. P. Skinner, in *Methods in Enzymology*, ed. S. Y. Tetin, Academic Press, 2013, pp. 139–166.
33 S. Y. Tetin, Q. Ruan and S. C. Saldana, *et al.*, Interactions of Two Monoclonal Antibodies with BNP: High Resolution Epitope Mapping Using Fluorescence Correlation Spectroscopy, *Biochemistry*, 2006, **45**(47), 14155–14165.
34 T. Nishikimi and Y. Nakagawa, Potential pitfalls when interpreting plasma BNP levels in heart failure practice, *J. Cardiol.*, 2021, **78**(4), 269–274.
35 R. Owczarzy, A. V. Tataurov and Y. Wu, *et al.*, IDT SciTools: a suite for analysis and design of nucleic acid oligomers, *Nucleic Acids Res.*, 2008, **36**(suppl_2), W163–W169.
36 P. C. Bevilacqua and J. M. Blose, Structures, kinetics, thermodynamics, and biological functions of RNA hairpins, *Annu. Rev. Phys. Chem.*, 2008, **59**(1), 79–103.
37 B. Li, Y. Jiang, X. Chen and A. D. Ellington, Probing Spatial Organization of DNA Strands Using Enzyme-Free Hairpin Assembly Circuits, *J. Am. Chem. Soc.*, 2012, **134**(34), 13918–13921.

